Multidomain Initiation Factor 2 from *Thermus thermophilus* Consists of the Individual Autonomous Domains[†]

Gabriel Žoldák,[‡,§] Erik Sedlák,[*,‡] Alexandra Wolfrum,[§] Andrej Musatov,[||] Diana Fedunová,[⊥] Karol Szkaradkiewicz,[§] and Mathias Sprinzl[§]

Department of Biochemistry, Faculty of Sciences, P. J. Šafárik University, Košice, Slovakia, Laboratorium für Biochemie, Universität Bayreuth, Bayreuth, Germany, Department of Biochemistry, The University of Texas Health Science Center, San Antonio, Texas 78229, and Department of Biophysics, Institute of Experimental Physics, Slovak Academy of Sciences, Košice, Slovakia

Received November 20, 2007; Revised Manuscript Received February 22, 2008

ABSTRACT: The three-dimensional chalice-like crystal structure of initiation factor 2 IF2/eIF5B from *Methanobacterium thermoautotrophicum* represents a novel fold and domain architecture in which the N-terminal G domain and the C-terminal C domain are separated by an ~40 Å α-helix. Homologous *Thermus thermophilus* initiation factor 2 (IF2wt), G (IF2G), and C (IF2C) domains were successfully overexpressed and purified which enabled us to perform a thermodynamic analysis and to asses the role of the domain architecture in this atypical fold. Circular dichroism in the far-UV region demonstrated that the proteins are well-folded and that the secondary structure content resembles that of IF2 from *M. thermoautotrophicum*. IF2wt and IF2G are monomeric proteins, while IF2C has a tendency to form dimeric species as shown by sedimentation velocity studies on analytical ultracentrifugation and differential scanning calorimetry scan analysis. Thermal denaturation studies of multidomain IF2wt reveals an exceptionally high reversibility (>90%) of the transition with a melting temperature of 94.5 °C. Melting temperature of IF2wt may be further increased in the presence of its physiological ligand GDP and the GTP analogue, GppNHp. The high reversibility of denaturation is achieved by the modular structure of the protein and by the high reversibility of the thermal denaturation of IF2G. On the other hand, hydrophobic IF2C aggregates during the thermal transition, and the aggregation is suppressed by guanidine hydrochloride. Isothermal denaturation demonstrates that both IF2G and IF2C have comparable stabilities of 46 and 33 kJ/mol, respectively. The apparent cooperative unfolding of the full-length protein has an unusually small denaturant *m* value. This together with the phase diagram method of analysis indicates the presence of intermediate(s) due to the independent unfolding of IF2G and IF2C. Despite an absence of apparent interactions between the domains in vitro, IF2G plays a role in IF2C reversibility in thermal denaturation. In conclusion, interactions between the domains of folded IF2wt in vivo are likely mediated by their α-helix connection and/or by a conformational change on the ribosome.

Translation initiation factor 2 (IF2)[1] is the largest nonribosomal protein factor involved in the initiation of protein biosynthesis in eubacteria and belongs to the family of structurally related enzymes that catalyze GTP hydrolysis during mRNA translation. In the course of the formation of the 70S ribosomal complex, IF2 interacts with numerous ligands, e.g., GTP and GDP, 30S and 50S ribosomal subunits, and fMet-tRNA^{fMet}. IF2 may also play a role in other cellular processes, such as transcription (*1*), protein secretion (*2*), protein folding (*3*), and function as a metabolic sensor (*4*).

The common sequence design of IF2 contains two distinctive parts: the diverse N-terminal region and the more conserved central and C-terminal segments (*5, 6*). Indeed, limited proteolysis of IF2 provides strong evidence for two structural and functional segments of the protein (*7, 8*). The N-terminal domain of IF2 is responsible for interaction with the 30S ribosomal subunit (*6*). The structural portion of IF2 harbors the GTPase activity and is know as the G-domain. The C-terminal domain is the part of IF2 responsible for the recognition of fMet-tRNA^{fMet} during translation initiation (*10*−*12*). Further thermodynamic and structural analysis of *Bacillus stearothermophilus* IF2 reveals the subdomain nature of the C-terminal domain (*13*−*15*). Although the mechanism

[†] We gratefully acknowledge financial support from the Deutsche Forschungsgemeinschaft (Grant Sp 243/12), from the Deutsche Akademische Austauschdienst (Grant D/01/02768), from Fonds der Chemischen Industrie and from the Slovak Grant Agency through Grant 1/3252/06, and from the Science and the Technology Assistance Agency (Grant APVT-20-006604).

* To whom correspondence should be addressed: Department of Biochemistry, Faculty of Science, P. J. Šafárik University, Moyzesova 11, 040 01 Košice, Slovakia. E-mail: erik.sedlak@upjs.sk.

[‡] P. J. Šafárik University.

[§] Universität Bayreuth.

[||] The University of Texas Health Science Center.

[⊥] Slovak Academy of Sciences.

[1] Abbreviations: IF2, initiation factor; IF2wt, intact full-length IF2 from *Thermus thermophilus*; IF2G, G-domain (residues 60–364) from *T. thermophilus*; IF2C, C-domain (residues 364–571) from *T. thermophilus*; CD, circular dichroism; DSC, differential scanning calorimetry; ΔASA_{unf}, change in accessible surface area of protein due to denaturation; ASA_{native}, accessible surface area of the protein in the native state; [GdnHCl], molar concentration of guanidine hydrochloride; *N*-ATA, *N*-acetyltryptophanamid.

10.1021/bi702295g CCC: $40.75
Published on Web 04/05/2008

of initiation of protein biosynthesis is different in prokaryotes and eukaryotes, there is a high level of sequence conservation among IF2 homologues from eubacteria, archaea, and eukaryotes. Biochemical evidence and sequence conservation among *Thermus thermophilus* IF2 and other IF2 homologues, including IF2/eIF5B from *Methanobacterium thermoautotrophicum*, indicate that all these proteins share a common domain organization (*16*−*18*). The sequence conservation is found among IF-2, EF-Tu, and EF-G, and it extends beyond the well-known homology of the nucleotide-binding domains (*19*).

Until now, efforts to crystallize intact IF2 were successful only in the case of IF2/eIF5B from *M. thermoautotrophicum* (*20*). The X-ray structure of *M. thermoautotrophicum* IF2/eIF5B reveals a novel and unusual chalice-like protein fold with two domains separated by an ~40 Å long α-helix. This fold, although atypical, possesses common properties with domain architectures of EF-Tu and EF-G, suggesting that all three proteins interact in a similar way with the ribosomal A-site (*20*). The study of the molecular architecture of the ribosome-bound IF2 as well as its structural model in solution reveals an expanded structure (*21, 22*). The presence of a flexible linker connecting N-terminal and central segments of the protein with the C-terminal domain (*23*) raises a question about the dynamic conformational transitions of IF2 in solution. Interestingly, the structure of release factor 2, another translation factor, differs in solution compared to the protein bound to the ribosome. While the solution structure of release factor 2 apparently corresponds to the compact crystal structure (*24, 25*), the interaction with the ribosome induces a conformational change from a compact to a largely expanded state (*26, 27*). In this work, we have meticulously elucidated the thermodynamic properties of IF2. The atypical chalice-like shape of the protein, indicating that domain dynamics may take place in solution, prompted us to perform a detailed thermodynamic analysis of intact IF2 along with its isolated domains.

MATERIALS AND METHODS

All chemicals were obtained from Sigma-Aldrich. All measurements were performed with protein samples dialyzed overnight against 50 mM sodium phosphate (pH 7.0). The concentration of proteins was determined with the molar extinction coefficients at 280 nm (*28*): $\epsilon = 25900\ M^{-1}\ cm^{-1}$ (IF2wt), $\epsilon = 9970\ M^{-1}\ cm^{-1}$ (IF2G), and $\epsilon = 15930\ M^{-1}\ cm^{-1}$ (IF2C). The concentration of guanidine hydrochloride (GdnHCl) was determined from refractive index measurements using the AR3-AR6 Abbe Refractometer (*29*).

Protein Purification and Preparation of Isolated Domains. IF2 from *T. thermophilus* was purified according to the protocol of Vornlocher et al. (*30*). The C-terminal domain (residues 364–571) (IF2C) and the G-domain (residues 60–364) (IF2G) of *T. thermophilus* IF2 were initially obtained by the preparative limited proteolysis of the intact protein with trypsin and thermolysin, respectively. The N-terminal segment (1–60) was found to have an unordered structure upon isolation and, thus, was not further analyzed. Digestion products were separated by the chromatography on a Q-Sepharose column (Pharmacia) (*11*). For expression of the C-terminal domain, the coding DNA sequence was amplified via PCR using the following primers: 5′-CAT ATG CAG GAG GAG GGG **CGT** AAG GAG CTC AAC C-3′ and 5′-G GAG CAT AAG CTT AGG CGG GGA CCT CC-3′ [*Nde*I and *Hin*dIII restriction sites are underlined; an AGG codon was changed into CGT (bold) for efficient expression in *Escherichia coli*]. For the overproduction of IF2G, the coding DNA sequence was amplified via PCR using the following primers: 5′-CAT ATG GCC AAG GTA **CGT** ATC-3′ and 5′-GGA TCC GGT CCG GGG GCG GCG-3′ [*Nde*I and *Bam*HI restriction sites are underlined; an AGG codon was changed into CGT (bold) for efficient expression in *E. coli*]. The resulting DNA fragments were cloned into pET28a (Novagen), and the corresponding polypeptides were expressed with an N-terminal His_6 tag in *E. coli* BL21(DE3) (Novagen). Nucleotide sequence was verified by sequencing. His_6-tagged IF2C and IF2G were purified by affinity chromatography on the Ni-NTA agarose (Qiagen). The His_6 tag was removed by digestion with thrombin, and the purified polypeptides were verified by N-terminal sequencing.

Circular Dichroism. Circular dichroism (CD) spectra were recorded in 50 mM sodium phosphate at 20 °C in JASCO J-600 or JASCO J-810 spectropolarimeters with 2–20 μM protein samples. Calibration of the instruments was performed using (1*S*)-(+)-10-camphorsulfonic acid. All CD spectra are averages of 6–16 consecutive scans. CD measurements in the far-UV region were performed with a bandwidth of 0.2 nm, a response time of 0.5 s, and a scan rate of 50 nm/min, using a rectangular cuvette with a path length of 1 mm. For the near-UV region, a rectangular cuvette with a path length of 1 cm was used. The cuvette holder was equilibrated at 20 °C by water circulation. Mean residue ellipticity [Θ] was calculated according to eq 1:

$$[\Theta] = \frac{M}{N_{res} - 1} \frac{\Theta_{obs}}{10dc} \quad (1)$$

where M is the molecular mass (63.19 kDa for IF2wt, 39.9 kDa for IF2G, and 23.4 kDa for IF2C), N_{res} is the number of residues (571 for IF2wt, 361 for IF2G, and 210 for IF2C), d is the path length in centimeters, c is the concentration in milligrams per milliliter, and Θ_{obs} is the measured ellipticity in millidegrees. The thermal transition was monitored by ellipticity at 220 nm. The temperature of samples was controlled by a Peltier element. The heating rate was 60 K/h.

The final CD spectrum, $\Theta_{G+C}(\lambda)$, reconstituted from the CD spectra of individual domains, $\Theta_G(\lambda)$ and $\Theta_C(\lambda)$, was calculated according to the equation

$$\Theta_{G+C}(\lambda) = \omega_G \Theta_G(\lambda) + \omega_C \Theta_C(\lambda)$$

where ω_G and ω_C are weighting factors for IF2G and IF2C, respectively. Mean residue ellipticity is averaged over the number of amino acids presented in the sequence. Therefore, the weighting factor is calculated as follows:

$$\omega_G = \frac{N_{res}(\text{G-domain})}{N_{res}(\text{wt})} = 0.63;\ \omega_C = \frac{N_{res}(\text{C-domain})}{N_{res}(\text{wt})} = 0.37$$

Guanidine Hydrochloride-Induced Unfolding. Isothermal denaturation was performed using guanidine hydrochloride (GdnHCl). The samples were incubated overnight. Circular dichroism and fluorescence measurements were performed using the same samples. The observed signal (S) was fitted into the following equation describing a two-state mechanism

and the linear dependence, m value, of the free energy $\Delta G°$ at 20 °C on the denaturant concentration, [D]:

$$S = \frac{S_{native} + b_{native}[D] + (S_{unfolded} + b_{unfolded}[D])e^{(-\Delta G° - m[D])/(RT)}}{1 + e^{(-\Delta G° - m[D])/(RT)}} \quad (2)$$

where S_{Native} and $S_{Unfolded}$ are signals for the native state and unfolded state without denaturant, respectively, and b_{Native} and $b_{Unfolded}$ are slopes for the native and unfolded states, respectively.

Fluorescence and Fluorescence Quenching. Fluorescence measurements were performed at 20 °C with 2–20 μM protein samples on a Perkin-Elmer LS-50B spectrometer with temperature control by water circulation or on a Shimadzu RF5000 spectrometer. Fluorescence quenching was performed using acrylamide, potassium iodide, and cesium chloride. Stock solutions of acrylamide, KI, and CsCl (4 M) were dissolved in 50 mM sodium phosphate (pH 7.0). After excitation at 295 nm, the tryptophan fluorescence (10 accumulations) was monitored at various quencher concentrations. Quenching of intrinsic tryptophans was analyzed according to eq 3 (*31*):

$$F_0/F = 1 + K_{SV}[Q] \quad (3)$$

where K_{SV} is the Stern−Volmer quenching constant in M^{-1}, [Q] is the concentration of the quencher (acrylamide, KI, or CsCl), and F_0 and F are the fluorescence in the absence and presence of the quencher, respectively.

Differential Scanning Calorimetry. DSC measurements were performed on the VP-DSC or DASM-4 instruments. Proteins were dialyzed overnight at 4 °C against 50 mM sodium phosphate (pH 7.0). Before and after thermal transition measurements, several buffer baselines were recorded to examine the signal reproducibility. Buffer and chemical baselines were subtracted from the calorimetric scans of proteins (*32*). Buffer and samples were degassed and stirred for 10 min at 15 °C. Samples were loaded into the DSC cells at room temperature. The scanning rate was 1 K/min, except for measurements of the scanning rate dependence. Calorimetric enthalpies of thermal transitions, ΔH_{cal}, were obtained after numerical integration of excess heat capacity. The van't Hoff enthalpy, ΔH_{vH}, was calculated simultaneously from the same calorimetric curve. The $\Delta H_{vH}/\Delta H_{cal}$ ratio provides information about the character of the thermal transition. If the transition is two-state type without aggregation of proteins, the ratio equals 1. In the presence of stable intermediates in the process of thermal denaturation, the ratio is less than 1. For a process with intermolecular cooperation, the ratio is greater than 1 and the value of the ratio is an estimation of the number of molecules in the cooperative units (*33*).

Analytical Ultracentrifugation. Sedimentation experiments were performed in the Center for Analytical Ultracentrifugation of Macromolecular Assemblies located in the Department of Biochemistry at the University of Texas Health Science Center. Sedimentation velocity studies were carried out in an Optima XL-I Beckman analytical ultracentrifuge in a four-hole AnTi-60 rotor. The rotor speed was 50000 rpm. Data were collected at 20 °C using optical absorption detection at 280 nm. The scans were analyzed by the method of van Holde-Weischet (*34*), using the UltraScan II version 9.3 data analysis software developed by B. Demeler (Department of Biochemistry, University of Texas Health Sciences Center). The data were corrected for buffer density and viscosity. The value for the partial specific volume of IF2 of 0.7404 cm^3/g and the value of 63195 Da for protein molecular mass were both calculated from the known amino acid sequence. The protein sample was dialyzed against 50 mM sodium phosphate buffer (pH 7.0) at 4 °C for 16 h. The initial IF2 concentration for sedimentation velocity experiments was 31 μM. One sample ("before thermal transition") was used without any other processing. The other sample ("after thermal transition") was heated from 20 to 100 °C with a constant heating rate of 1 °C/min and, subsequently, allowed to cool at room temperature and used for the sedimentation velocity experiment.

RESULTS

On the basis of similarities in the primary structure of *T. thermophilus* and *M. thermoautotrophicum* proteins (Figure 1A), a hypothetical model of *T. thermophilus* IF2 was constructed (Figure 1B) using an automatic web service 3D jigsaw ((35–37); http://www.bmm.icnet.uk/servers/3djigsaw/).This model shows similarities to *M. thermoautotrophicum* IF2/eIF5B structure (Figure 1a,b). However, it must be taken very carefully into consideration, since the chalice-like fold is a very rare case in structural databases and may lead to bias.

Circular Dichroism Spectra of IF2wt, IF2G, and IF2C. CD spectra of IF2wt, IF2G, and IF2C were measured in the far- and near-UV regions, both in the absence and in the presence of 7 M GdnHCl (Figure 2). CD in the far-UV region is a practical method for assessing the secondary structure of proteins in solution. Far-UV CD measurements showed that both intact protein and isolated domains have well-defined secondary structures. Strong signals in the near-UV region revealed the presence of the asymmetrical environment of aromatic residues. Thus, IF2wt, as well as its individual domains, possesses folds with well-defined and properly packed secondary and tertiary structures.

In the far-UV region, both IF2wt and IF2G possess two pronounced minima typical of the polarized $\pi \rightarrow \pi^*$ (at 208 nm) and $n \rightarrow \pi^*$ (at 222 nm) electronic transitions of the α-helix. Only one minimum characteristic for β-sheets (at 215 nm) is observed in the spectrum of IF2C. We used these spectra for assessment of the secondary structure of the full-length protein and isolated domains. Spectral analysis was performed with CDSSTR available on the DICHROWEB website (*37, 38*). The quality of the results and the goodness of the fit were quantified via NRMSD parameters (*39*). Calculated and observed CD spectra of the protein and its domains are very similar (Figure 2) with NRMSD values indicating an average error of <5% between the fitted and the experimentally measured CD spectra. The predicted secondary structures indicate that IF2wt contains 31% α-helix, 22% β-sheets, 19% turns, and 27% nonregular regions. IF2G contains 23% α-helix, 24% β-sheets, 21% turns, and 32% nonregular regions. IF2C contains 18% α-helix, 33% β-sheets, 22% turns, and 28% nonregular regions. Secondary structure predictions and their variance from the analysis of CD spectra are summarized in the Supporting Information.

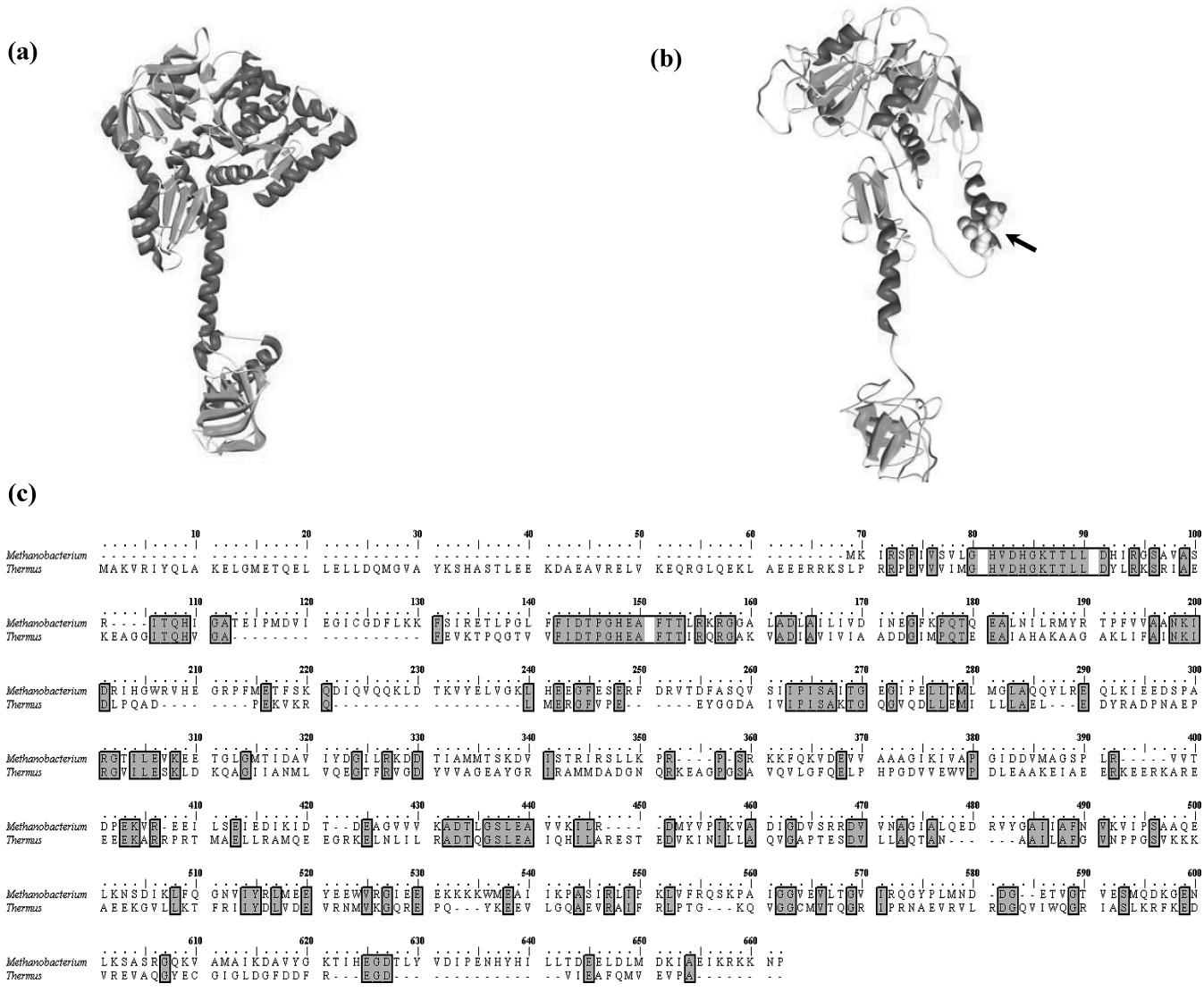

FIGURE 1: (A) Three-dimensional (3D) structure of IF2 from *M. thermoautotrophicum* [Protein Data Bank (PDB) entry 1g7t] and (B) model of IF2 from *T. thermophilus*. (C) Sequence alignment of IF2s from *M. thermoautotrophicum* and *T. thermophilus*. The 3D model was made by using automatic web service 3D jigsaw ((34, 35); http://www.bmm.icnet.uk/servers/3djigsaw/). Sequence alignment was performed using ClustalW. Identical residues are boxed. The arrow indicates the putative boundary between the G- and C-domains.

The signals in the near-UV region result from the contribution of aromatic residues and disulfide bridges. *T. thermophilus* IF2 possesses two tryptophans (W325 and W522), 10 tyrosines, 14 phenylalanines, and two cysteines (C499 and C545), which may contribute to the near-UV signals (Figure 2). The rotatory strength of the CD band in the near-UV region is the strongest for the full-length protein. Reconstitution of the IF2wt spectrum from the weighted spectra of the isolated domains reveals the lower intensity of the reconstituted spectrum. Tryptophans are equally distributed between IF2G and IF2C. In IF2G, there are seven tyrosines, seven phenylalanines, and no cysteines. In IF2C, there are three tyrosines, seven phenylalanines, and two cysteines. The sequence alignment of the whole protein shows that positions of the aromatic residues and cysteines are not the same as in *M. thermoautotrophicum* IF2 (Figure 1). This precludes their structural colocalization. In the presence of 7 M GdnHCl, disappearance of the signal in the near-UV region indicates unfolding of the packed tertiary structure (Figure 2).

IF2wt and the isolated domains were unfolded in the presence of 7 M GdnHCl (Figure 2). The intensities of the CD bands at 222 nm were low, i.e., –29.8, –635, and –776 deg cm^2 dmol^{-1} for IF2wt, IF2G, and IF2C, respectively. Analysis of the major backbone conformation of the unfolded proteins showed that polyproline II (P_{II}) conformation is present at a significant level (*40*). The P_{II} helix content can be estimated from the model peptide experiments (*41, 42*) to be as high as 37, 33, and 32% for IF2wt, IF2G, and IF2C, respectively. These values indicate that at room temperature, approximately one-third of the backbone conformation is presented in the P_{II} conformation and the rest in the unordered form, in agreement with previous findings (*40*).

Isothermal Denaturation of IF2wt and Its Domains. Urea was an ineffective denaturant. Even at 9 M, urea did not perturb the secondary structure of IF2wt (data not shown). GdnHCl was used to induce unfolding of IF2wt, IF2G, and IF2C (Figure 3). Fluorescence of intrinsic tryptophans, changes in emission maxima (emission at a fixed wavelength, i.e., 350 nm; Figure 1S of the Supporting Information), and ellipticity in the far-UV region were chosen to monitor protein unfolding (Figure 3). These techniques are independent of each other and allow the analysis of unfolding at different structural levels. The combination of fluorescence

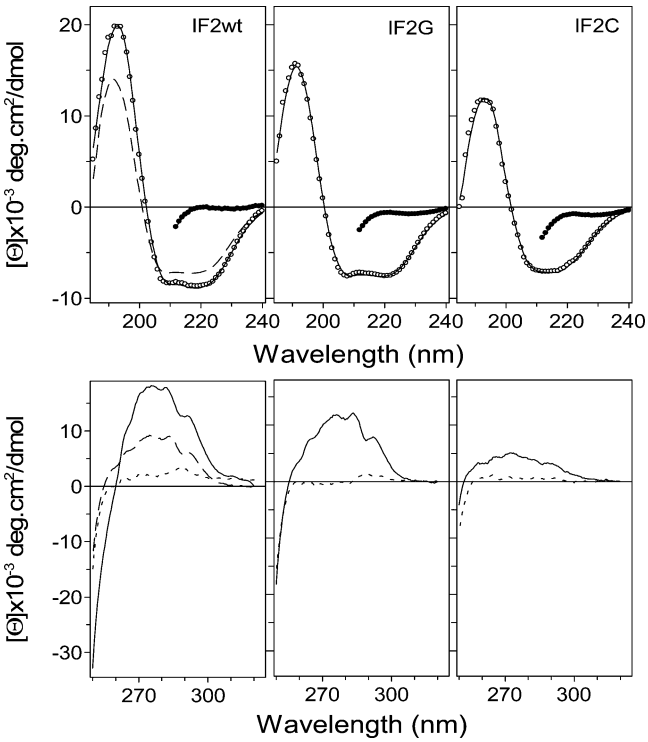

FIGURE 2: CD spectra of native and unfolded IF2wt, IF2G, and IF2C in the far-UV (top panels) and near-UV regions (bottom panels). In the top panels are shown CD spectra of the native proteins (○) and unfolded proteins in 7 M GdnCl (●) in the peptide region. Solid lines are theoretical curves obtained from the CDSSTR algorithm. The dashed lines represent weighted sums of the CD spectra of individual domains. The number of accumulated spectra was 6–10. In the bottom panels are shown CD spectra of the native proteins (solid lines) and unfolded proteins in 7 M GdmCl (dotted lines) in the near-UV region. Dashed lines represent weighted sums of CD spectra of individual domains. The protein concentration was 15–20 μM. The number of accumulated spectra was 20. All measurements were performed in 50 mM sodium phosphate (pH 7.0) at 20 °C.

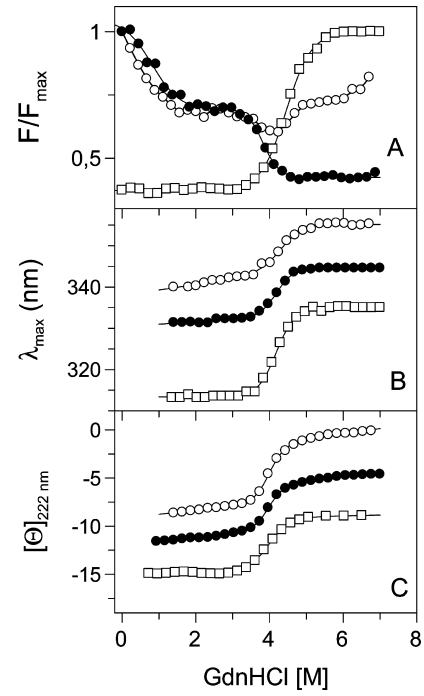

FIGURE 3: GdnHCl-induced isothermal denaturation of IF2wt (○), IF2G (●), and IF2C (□) monitored by (A) fluorescence, (B) emission shift, and (C) protein ellipticity in the far-UV region at 222 nm. (A) The curves passing the points are only guides for the eye. (B) For clarity, emission maxima are shifted by −10 nm for IF2G and −20 nm for IF2C. The curves passing the points are only guides for the eye. (C) For clarity, ellipticites at 222 nm are shifted by −4 units for IF2G and −8 units for IF2C. The curves passing the points are based on nonlinear curve fitting of eq 2 in Materials and Methods. The protein concentration was between 2 and 20 μM. All measurements were performed in 50 mM phosphate buffer (pH 7.0) at 20 °C.

and the far-UV CD measurements provides independent monitoring tools of local and global conformational changes.

The fluorescence of IF2wt shows complex trends: fluorescence intensity decreases at <2.0 M GdnHCl, and a further decrease occurs until 4 M GdnHCl followed by an increase at higher GdnHCl concentrations (Figure 3A). The decrease in the fluorescence at <2.0 M GdnHCl is not caused by an increased ionic strength. Control titrations indicate that the fluorescence of IF2wt was nearly independent of the ionic strength in the range of 0–2 M NaCl. Free energy changes and *m* values could not be evaluated because of the complex trend in the tryptophan fluorescence of IF2wt. As shown below, the complex effects of the GdnHCl concentration on IF2wt fluorescence reflect changes in the intrinsic tryptophan fluorescence induced by the independent unfolding of domains.

The fluorescence-monitored GdnHCl-induced unfolding of IF2G at low denaturant concentrations (<2 M) shows the decrease in tryptophan fluorescence in a manner similar to that of IF2wt and can be described by the following parameters: $\Delta G° = 5.4 \pm 1.6$ kJ/mol and $m = 6.6 \pm 1.3$ kJ mol^{-1} M^{-1}. At higher concentrations of GdnHCl, fluorescence decreases in a sigmoidal way and data are described as follows: $\Delta G° = 43.5 \pm 3.8$ kJ/mol and $m = 11.4 \pm 1.0$ kJ mol^{-1} M^{-1}. The fluorescence of IF2C increases upon unfolding and was analyzed by nonlinear curve fitting (eq 2). Data are described by the following parameters: $\Delta G° = 33.0 \pm 1.5$ kJ/mol and $m = 7.5 \pm 0.3$ kJ mol^{-1} M^{-1}.

The polarity and dynamics of the nearby tryptophan environment were dramatically changed upon GdnHCl-induced protein unfolding. The emission maximum is a very sensitive probe for monitoring these changes (Figure 3B). The emission maximum of IF2wt fluorescence was shifted from 339 nm in the buffer without denaturant to 350 nm in the presence of 7 M GdnHCl. In the case of IF2G and IF2C, similar shifts from 339 to 355 nm and from 334 to 355 nm were observed, respectively. The largest emission shift in tryptophanyl residue fluorescence was observed in the case of IF2C, indicating its hydrophobic environment. In unfolded states, emission maxima were comparable with that of free *N*-ATA in solution (355 nm). Noteworthy is the fact that in the presence of 9 M urea the emission maxima are at ~338–340 nm for the full-length protein and isolated domains. Sigmoidal changes in emission maxima may be analyzed in terms of $\Delta G°$ and *m* only in the case of the equal fluorescence intensity of the native and unfolded states. In other cases, observed emission maxima are weighted both by the population of native and unfolded conformations and by the intensities of these forms. Therefore, the emission spectral shifts were not analyzed.

Secondary structure unfolding of IF2wt was analyzed by the two-state mechanism (Figure 3C). Data were described by the following parameters: $\Delta G° = 47.0 \pm 2.9$ kJ/mol and

$m = 11.8 \pm 1.0$ kJ mol^{-1} M^{-1}. Unfolding of IF2G was described by the following parameters: $\Delta G° = 46.1 \pm 2.5$ kJ/mol and $m = 11.6 \pm 0.6$ kJ mol^{-1} M^{-1}. GdnHCl-induced unfolding of IF2C was described by the following parameters: $\Delta G° = 33.1 \pm 1.5$ kJ/mol and $m = 8.4 \pm 0.4$ kJ mol^{-1} M^{-1}. Remarkably, the m value is significantly smaller than the sum of the m values for the individual domains.

Unfolding of the Isolated Domains Reveals the Presence of Equilibrium Intermediates. The fluorescence study of the individual domains provided insight into the complex nature of IF2wt unfolding and offered an explanation for the absence of sigmoidal unfolding dependence. Unfolding of IF2G in the presence of GdnHCl showed biphasic character. (1) The first transition leading to the first intermediate with the native-like secondary structure was accompanied by a sigmoidal decrease in the tryptophan fluorescence at low concentrations (<2.5 M). The m value of this transition is 6.6 kJ mol^{-1} M^{-1}, and recalculation of ΔASA_{unf} led to a value of 3300 Å^2. This conformational transition is relatively small and was not observed at the level of secondary structure. No transition was observed in the control titration with NaCl, indicating that the observed effects were not due to the increased ionic strength. (2) The second transition was accompanied by a sigmoidal decrease in both tryptophan fluorescence and ellipticity at 222 nm. Fluorescence and ellipticity dependences were described by similar m values: 11.4 and 11.6 kJ mol^{-1} M^{-1}, respectively. Two independent experimental techniques used to monitor different parts of the structure indicated that at high concentrations of GdnHCl (>3.0 M) IF2G unfolding might be described by a two-state mechanism.

Isothermal unfolding of tertiary and secondary structures of IF2C was characterized by single sigmoidal transitions. Unfolding curves of secondary and tertiary structures did not overlap, indicating a non-two-state transition (*43*). The secondary structure unfolding was described by a $\Delta G°$ of 33.1 kJ/mol and an m of 8.4 kJ mol^{-1} M^{-1} and was followed by unfolding of the tertiary structure described by a $\Delta G°$ of 33.0 kJ/mol and an m of 7.5 kJ mol^{-1} M^{-1}. Standard deviations of parameters obtained from the nonlinear regression and from repeating experiments revealed that the shift in unfolding curves was statistically significant. We conclude that unfolding of IF2C was at least a three-state reaction.

The complexity of isothermal unfolding of IF2 and its domains was also analyzed by using phase diagram methods (*44*−*46*). The basis of this powerful method in revealing hidden intermediates is a pairwise correlation of two different extensive parameters (e.g., spectral intensities) in a plot. For the two-state transition, the plot of the intensities should be linear. Any nonlinearity corresponds to the deviation from an all-or-none transition. The number of linear portions, n, indicates $n + 1$ species. This phase diagram method should be applied to data measured under identical conditions. Here, fluorescence emission intensities at 320 and 365 nm (upon excitation at 295 nm) were interrelated and plotted as F_{320} versus F_{365} (Figure 4). Clearly, the spectral diagrams are not linear, indicating the presence of intermediates and/or partially unfolded states. There are four linear regions which indicate at least five species. Four of them could be assigned within the context of the simple two-domain model (N, native; U, unfolded), NN, NU, UN, and UU, and other intermediate(s) might be a result of

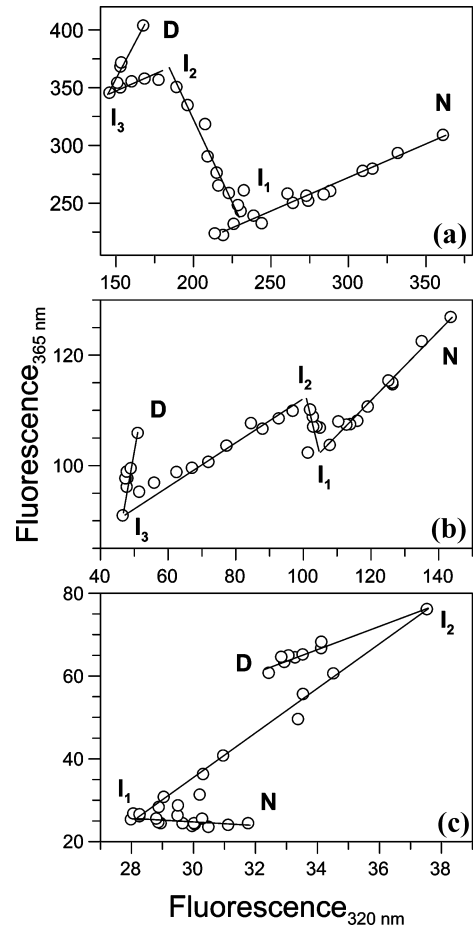

FIGURE 4: Phase diagram method analysis of isothermal denaturation of IF2wt (A), IF2G (B), and IF2C (C) monitored by fluorescence emission intensities at 320 and 365 nm (upon excitation at 295 nm). The phase diagrams indicate the presence of three, three, and two intermediates in isothermal unfolding of IF2wt, IF2G, and IF2C, respectively.

perturbation of the multidomain nature (domain interfaces) within G- and C-domains. Interestingly, phase diagrams of the individual G- and C-domains indicate the presence of, at least, three and two intermediates, respectively. This indicates either an existence of hidden intermediates (that even the phase diagram plot is not able to reveal) when the domains are part of intact IF2 or destabilization of multidomain structures of isolated G- and C-domains. The latter points to a possible stabilization effect of connecting α-helical structure for G- and C-domains.

Thermal Denaturation of IF2wt, IF2G, and IF2C Monitored by CD. Thermal denaturation of the secondary structure of IF2wt was monitored by CD in the far-UV region. The ellipticity changes were followed at 222 nm (Figure 5A). In the absence of GdnHCl, the transition temperature was >95 °C. Such a high transition temperature and the observed slopes of the pre- and post-transition regions hampered reliable thermodynamic analysis. Addition of GdnHCl decreased both transition temperatures and enthalpies of transition (Figure 8 and Table 2A of the Supporting Information). At high temperatures, ellipticities of the thermally denatured state were gradually changed by increased concentrations of denaturant up to 2.5 M GdnHCl. At higher GdnHCl concentrations, the ellipticities of thermally denatured IF2wt were comparable with those measured in the presence of 7 M GdnHCl. A temperature-dependent decrease

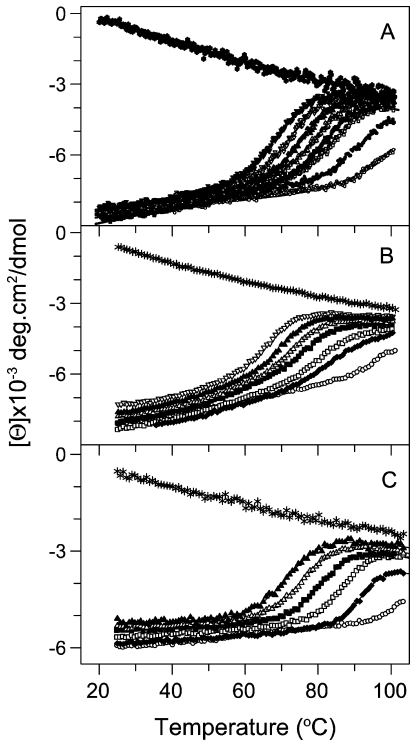

FIGURE 5: Thermal denaturation of (A) IF2wt, (B) IF2G, and (C) IF2C monitored by CD in the far-UV region at various concentrations of GdnHCl: (A) 0 (○), 0.95 (●), 1.7 (□), 1.9 (■), 2.13 (△), 2.4 (▲), 2.6 (▽), 2.84 (▼), and 7 M GdnHCl (★), (B) 0 (○), 1.87 (●), 2.33 (□), 2.8 (■), 3.03 (△), 3.27 (▲), 3.5 (▽), and 7 M (★), and (C) 0 (○), 1.63 (●), 2.1 (□), 2.57 (■), 3.03 (△), 3.27 (▲), and 7 M (★). Curves passing experimental points were obtained from a nonlinear fitting procedure, except for the 0 and 7 M GdnHCl curves that are only guides for the eye. The protein concentration was between 2 and 20 μM. All measurements were performed in 50 mM phosphate buffer (pH 7.0). The scan rate was 1 °C/min.

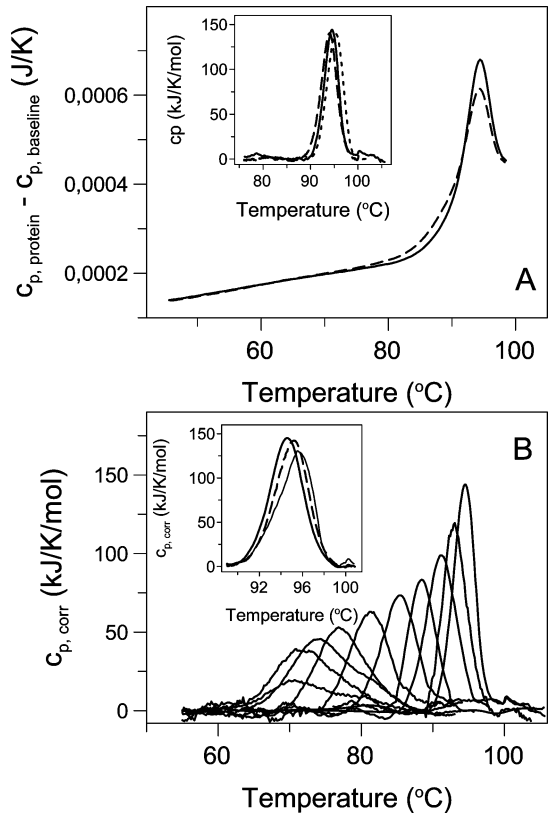

FIGURE 6: Thermal denaturation of IF2wt measured by DSC. (A) Calorimetric traces of the protein upon baseline subtraction (joules per kelvin): first and second heating (solid and dashed line) at a scanning rate of 1 K/min. The inset shows DSC traces at various scan rates: 0.5 (---), 1 (—), and 2 K/min (———). (B) DSC scans (in kilojoules per kelvin per mole) of the protein in the presence of various concentrations of GdnHCl. From right to left, GdnHCl concentrations were 0, 0.25, 0.5, 0.75, 1.0, 1.5, 2.0, 2.5, 2.75, and 3.0 M. The inset shows DSC traces of the protein without nucleotide (thick solid line), in the presence of 1 mM GDP (dashed line), and in the presence of 1 mM GTP (thin solid line). The protein concentration was between 10 and 50 μM. All measurements were performed in 50 mM phosphate buffer (pH 7.0).

in ellipticity of the unfolded state (in 7 M GdnHCl) is generally observed and is consistent with the view of the conformational energetics of the polypeptide conformations (*47, 48*). The presence of the negative slope is in agreement with the proposal that the polyproline P_{II} conformation is the most energetically stable conformation (ground state) of the polypeptide chain. Thermal denaturation of IF2wt was also monitored in the near-UV region at 275 nm. These measurements allowed us to monitor denaturation by local probes, aromatic residues (data not shown). Furthermore, ellipticity changes due to the thermal denaturation at various GdnHCl concentrations were also monitored for IF2G and IF2C (Figure 5B,C). Transition temperatures obtained from these measurements are summarized in Figure 9. Differences in ellipticities at 222 nm, observed in the absence and presence of GdnHCl, indicate distinctions that exist between thermally denatured states.

Thermal Denaturation of IF2wt Monitored by Differential Scanning Calorimetry. Differential scanning microcalorimetry (DSC) experiments were performed with various protein and GdnHCl concentrations in the presence and absence of physiological IF2 ligands, GTP and GDP (Figure 6). Unexpectedly, IF2, being a large multidomain protein, displayed only a single endothermic peak in the profile of the thermally induced denaturation. The transition temperature (T_{trs}) of IF2wt has a relatively high value of 94.5 °C. The calorimetric enthalpy (ΔH_{cal}) calculated directly from the scan was ~560 kJ/mol. Noteworthy is the fact that the calorimetric enthalpy calculated in this way is model-independent and assumption-free, as opposed to the van't Hoff enthalpy based on the reversible two-state model.

Thermal denaturation followed by CD in the far- and near-UV regions revealed reversibility of the CD spectra upon cooling of the sample. This effect indicates nearly complete recovery of the secondary structure elements and recovery of the global tertiary structure. DSC experiments further confirmed the denaturation reversibility of IF2. When the first heating was immediately stopped after thermal transition, the second heating scan showed 90% reversibility of the single denaturation peak (Figure 6A). For the analysis, the protein was heated to 115 °C. As expected, the reversibility of the thermal transition was dependent on the final temperature of the DSC measurements. However, even heating to 130 °C decreased the reversibility of the thermal transition only to ~50%. Irreversible denaturation becomes more pronounced at temperatures above the transition temperature.

Prior to the equilibrium thermodynamics analysis, several test experiments were performed at various scanning rates. A test of scanning rate dependence is greatly important for validation of the application of equilibrium thermodynamics

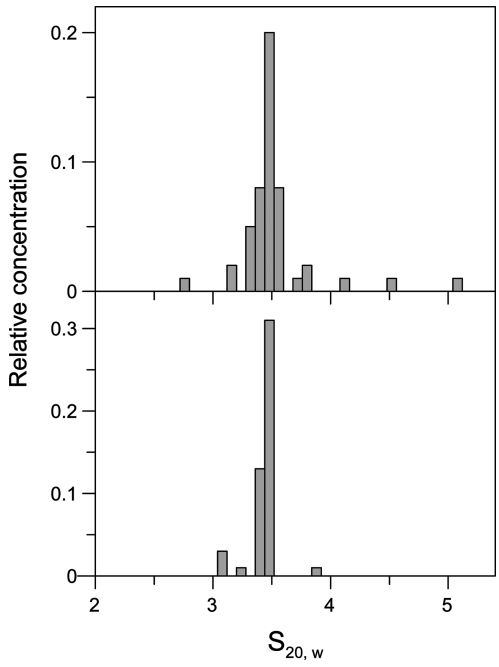

FIGURE 7: Distribution of sedimentation coefficients, $s_{20,w}$, of IF2wt before (top panel) and after (bottom panel) thermal denaturation. Similar average sedimentation coefficients for both samples strongly indicate the monomeric form of IF2wt both before and after thermal denaturation. Data were collected at 20 °C using optical absorption detection at 280 nm. The data were corrected for buffer density and viscosity.

to the given set of measurements (*49*). Thermal denaturation of IF2wt measured at scanning rates of 0.5 and 2 K/min differed by less than 1 °C in transition temperature (inset of Figure 6A). In both cases, the extent of the reversibility was nearly the same, indicating that the observed small temperature transition shift was most likely caused by a slow protein relaxation during DSC measurements.

The functional cycle of IF2 includes changes in the nucleotide status between the GDP- and GTP-bound form of the protein (*20*). The effect of the presence of 1 mM GDP and 1 mM GTP on the thermal denaturation of the protein was analyzed by DSC (inset of Figure 6B). Addition of GTP or GDP led to a slight increase in the T_{trs} to 95.2 or 95.6 °C, respectively. The scan in the presence of GDP became asymmetric most likely due to a differential ligand-induced stabilization of domains. To test this possibility, GdnHCl was used to destabilize possible domain−domain interactions. Increasing the denaturant concentration led to a decrease in transition temperature with the appearance of asymmetry in the scans with a GdnHCl concentration of >2 M (Figure 6B). Reversibility of these transitions in the presence of GdnHCl was retained. Thermodynamic parameters obtained from DSC experiments with IF2wt in the presence of GdnHCl in the range of 0−2 M are summarized in Table 2 of the Supporting Information; the dependence of transition temperatures obtained by CD and DSC is shown in Figure 9A. Surprisingly, at the protein concentration of ~50 μM when $T = T_{trs}$, the $\Delta H_{vH}/\Delta H_{cal}$ ratio equaled 2.0 ± 0.1, indicating that the dimer is the cooperative unit in the process of thermal denaturation of full-length IF2.

Analytical Ultracentrifugation of IF2wt. To reveal the formation of the dimer of IF2wt indicated by the DSC results, analytical ultracentrifugation experiments were performed. A preparation of IF2wt, in standard low-ionic strength buffer

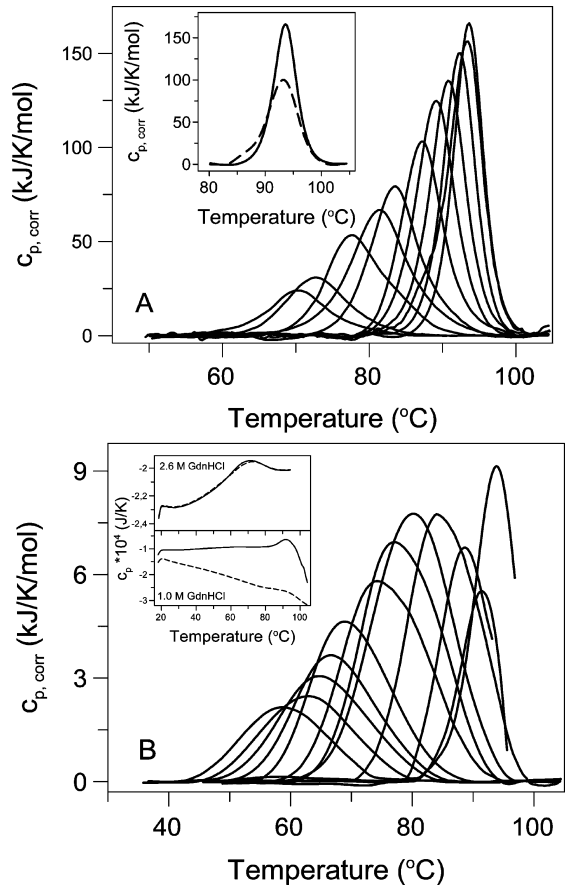

FIGURE 8: Thermal denaturation of (A) IF2G and (B) IF2C monitored by DSC at various concentrations of GdnHCl. (A) Thermally induced denaturation of IF2G in the presence of various GdnHCl concentrations (from right to left): 0, 0.25, 0.5, 0.75, 1.0, 1.25, 1.5, 1.75, 2.0, 2.5, 3.0, and 3.5 M. The inset shows, first, the baseline-corrected scan (—) and, second, the rescan (– – –) in 50 mM sodium phosphate buffer (pH 7.0). (B)Thermally induced denaturation of IF2C in the presence of GdnHCl concentrations (from right to left): 0, 0.8, 1.0, 1.2, 1.6, 2.0, 2.2, 2.4, 2.6, 2.8, 3.0, 3.2, and 3.6 M. The inset shows, first, the scan (—) and, second, the rescan (– – –) of IF2C in the presence of 1.0 M GdnHCl (bottom panel of the inset) and 2.6 M GdnHCl (top panel of the inset). The protein concentration was between 2 and 20 μM. All measurements were performed in 50 mM phosphate buffer (pH 7.0). The scan rate was 1 °C/min.

[50 mM phosphate buffer (pH 7.0) at 20 °C] was found to be homogeneous as analyzed by sedimentation velocity. The protein had an $s_{20,w}$ of 3.4–3.6 S [with an average of 3.53 S (Figure 7, top panel)]. The distribution of sedimentation coefficients of IF2wt was unaffected by thermal denaturation. The sedimentation coefficient $s_{20,w}$ of 3.47 (average) for thermally denatured IF2wt shows a value very similar to that originally obtained for the untreated protein (Figure 7, bottom panel). Such similarity of $s_{20,w}$ unambiguously allows us to conclude that thermal denaturation does not induce aggregation of IF2wt.

A self-association state, i.e., dimeric or monomeric nature of IF2 in vitro, was also examined using $C(s)$ analysis according to the method of Schuck (*50*). With this approach, self-association is analyzed by fitting sedimentation velocity data to the Lamm equation (*51*−*53*). Therefore, the molecular weights of IF2wt, before and after thermal denaturation, were evaluated from the computer fitting of experimental sedimentation data. The generated best fits result in a molecular weight of 52000 ± 2000, suggesting that IF2wt is monomeric.

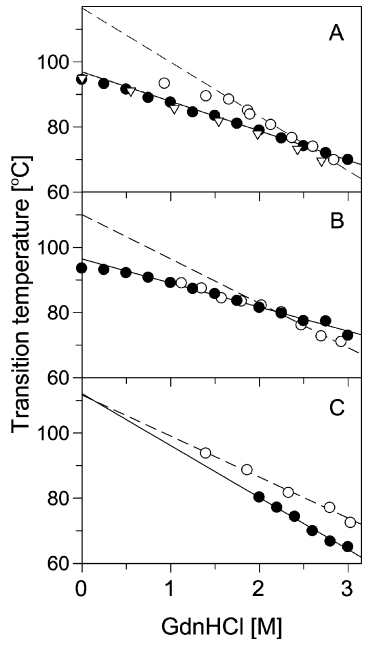

FIGURE 9: Transition temperatures of (A) IF2wt, (B) IF2G, and (C) IF2C, obtained from measurements performed by DSC (●) and by CD in the far-UV (○) and near-UV (▽) regions.

Thermal Denaturation of IF2G and IF2C Monitored by DSC. DSC was also used to monitor the thermal denaturation of IF2G and IF2C at various GdnHCl concentrations (Figure 8A). Thermal denaturation of IF2G in the absence of GdnHCl showed a single cooperative transition with a T_{trs} of 93.5 °C and a ΔH_{cal} of 836 kJ/mol. The second heating exhibited an endothermic peak indicating ~80% reversibility of the thermal denaturation (inset of Figure 8A). This reversibility depended strongly on the highest temperature achieved during scanning and could be increased by stopping the DSC measurement at temperatures no more than 5 °C higher than the transition temperature. Addition of GdnHCl led to a decrease in the transition temperatures and calorimetric enthalpies. At GdnHCl concentrations of >2 M, DSC scans became more asymmetric and more prolonged at the high-temperature side. Any aggregation of IF2G could not be observed under the experimental conditions that were used. Observed effects were not caused by the irreversibility of the transition but most likely were due to the multistate nature of the thermal denaturation since IF2G consists of at least three subdomains. Enthalpies of transition and transition temperatures of DSC thermal denaturation of IF2G at various GdnHCl concentrations are summarized in the Supporting Information (Table 2B). The dependence of transition temperatures obtained by CD and DSC is shown in Figure 9B. The $\Delta H_{vH}/\Delta H_{cal}$ ratio equaled ~1.0 in the range of GdnHCl concentrations of 0–2 M, indicating that the monomer was the cooperative unit of IF2G in the process of thermal denaturation.

The measurement and analysis of the thermal denaturation behavior of IF2C in the absence of GdnHCl were problematic due to massive protein aggregation. Addition of GdnHCl suppressed IF2C aggregation at concentrations of >1 M (Figure 8B). The reversibility of the thermal transition was markedly improved above 2 M GdnHCl and achieved nearly 100% efficiency at 2.8 M GdnHCl (inset of Figure 8B). Transition temperatures decreased in the presence of GdnHCl. The enthalpy of transition could be analyzed only at GdnHCl concentrations higher than 2 M. The $\Delta H_{vH}/\Delta H_{cal}$ ratio equaled ~2 at GdnHCl concentrations of >2 M, indicating that the dimer is the cooperative unit of IF2C in the process of thermal denaturation. In fact, dimer formation of IF2C in the thermal denaturation was further supported by analytical ultracentrifugation findings (Figure 3S of the Supporting Information). The transition profile became asymmetric at high denaturant concentrations. Enthalpies and transition temperatures of thermal denaturations of IF2C measured at various GdnHCl concentrations are summarized in Table 2C (Supporting Information), and the dependence of transition temperatures obtained by CD and DSC is shown in Figure 9C.

Comparison of Thermal Transitions of Secondary and Tertiary Structures of IF2wt, IF2G, and IF2C. Transition temperatures of thermal transitions for IF2wt and the isolated domains in the presence of various GdnHCl concentrations are shown in Figure 9. GdnHCl concentration dependences of transition temperatures obtained by DSC were for all proteins linear with a slight curvature at low GdnHCl concentrations in the case of IF2wt and IF2G. The observed nonlinearity was very likely an effect of ionic strength on the stability of the studied proteins. Linear extrapolations of these dependences to 0 M GdnHCl led to T_{trs} values of 96.9 ± 0.2, 97.0 ± 0.8, and 112.1 ± 2.1 °C for IF2wt, IF2G, and IF2C, respectively. On the other hand, dependences of T_{trs} on GdnHCl concentration, obtained by CD measurements, are more complex. In the case of IF2C, this dependence is linear with the temperature extrapolated at 0 M (T_{trs} = 111.6 ± 2.1 °C). This value is similar to that obtained by DSC, yet dependences for IF2wt and IF2G can be divided into two linear regions. There is an apparent break at a GdnHCl concentration of 1.7 M in the linearity of the dependence for IF2wt. Extrapolation in the region at <1.7 M GdnHCl leads to a T_{trs} of ~97.5 °C, i.e., a value close to that obtained by DSC, while extrapolation at >1.7 M GdnHCl leads to a T_{trs} of ~116.5 °C. An analogous procedure leads to a T_{trs} of ~97.0 °C at <2.0 M GdnHCl and a T_{trs} of ~110.0 °C at >2.0 M GdnHCl in the case of IF2C.

DISCUSSION

Comparison of Structures of IF2 from T. thermophilus and M. thermoautotrophicum. Until now, no three-dimensional structure of any intact prokaryotic IF2 had been determined. Structures of the isolated N-terminal subdomain (PDB entry 1nd9) from *E. coli* and the C-terminal subdomain C1 (PDB entry 1d1n) as well as fMet-tRNA^{fMet} -binding subdomain C2 (PDB entry 1z9b) from *B. stearothermophillus* were determined by NMR (*14, 15, 54*). There are also models of *E. coli* and *T. thermophilus* IF2 bound to the ribosome based on cryo-electron microscopy (PDB entry 1z01) (*55, 56*).

The sequence of *M. thermoautotrophicum* IF2 is 23% identical, in a pairwise fashion, with that of *T. thermophilus* IF2, the highest value among all eubacterial IF2 homologues (Figure 1). The three-dimensional structure of IF2/eIF5B from *M. thermoautotrophicum* consists of four domains arranged in the form of the long molecular chalice (*20*) (PDB entry 1g7t). The G-domain (residues 1–225), domain II (residues 231–327), and domain III (residues 344–445) are grouped and held together by the intradomain contacts and by partial burying in the surface. The C-terminal domain

(residues 462–550) is separated from domains I−III by a 40 Å long stem. According to the X-ray structure, there are no domain−domain contacts between the C-terminal domain and any other domains of IF2. The C-terminal domain of IF2/eIF5B and C-terminal subdomain C2 from *B. stearothermophillus* IF2 are arranged in the form of a β-barrel. The sequence of the C-terminal domain of *T. thermophilus* IF2 has a very high level of identity (54%) with that of C-terminal subdomain C2 of *B. stearothermophillus* IF2, indicating their similar fold.

Secondary Structure Contents of the Initiation Factors Are Similar. Results obtained with CD spectroscopy of *T. thermophilus* IF2 can be compared with the three-dimensional structure of *M. thermoautotrophicum* IF2/eIF5B, which served as the basis for the *T. thermophilus* IF2 model (*20*) [PDB entry 1g7t (Figure 1)]. *M. thermoautotrophicum* IF2/eIF5B contains 30% α-helix, 29% β-sheets, 13% turns, and 28% nonregular regions. These values are consistent with the percent fractions of the secondary structure elements predicted from the CD spectra of *T. thermophilus* IF2. Calculation of the secondary structure content of the G-domain and the C-terminal domain of *M. thermoautotrophicum* IF2/eIF5B was performed for residues 1–445 and 445–569, respectively. According to this calculation, the G-domain contains 33% α-helix, 26% β-sheets, 12% turns, and 29% nonregular regions and the C-terminal domain contains 22% α-helix, 29% β-sheets, 17% turns, and 32% nonregular regions. The values are close to the values obtained from the measured CD spectra of the isolated domains of *T. thermophilus* IF2.

In addition, CD spectra of the full-length protein were compared to the weighted sum of the CD spectra of the individual domains. The observed CD spectrum of IF2wt is not the same as the CD spectrum calculated from weighted CD spectra of the isolated domains, indicating slight perturbation in the secondary structure of domains due to dissection of full-length IF2 (Figure 2) and the absence of the short helical part at the N-terminus (residues 1–60). This part is unfolded upon isolation; however, within the protein structure, it forms a helical structure.

Presence of Intermediates in the Isothermal Denaturation of T. thermophilus IF2 and Its Domains. Fluorescence and CD analysis of the isothermal denaturation of *T. thermophilus* IF2 and its domains revealed multidomain structures (Figure 3). Noteworthy is the fact that the *m* value of 11.78 kJ mol^{-1} M^{-1}, obtained from the slope of the linear dependence of the free energy of unfolding on the denaturant concentration, is significantly lower than the expected theoretically assessed value (*57*) and indicates the presence of a transition intermediate(s). The change in the accessible surface area predicted for all residues of full-length IF2 equals 52196 Å^2 and yields the an *m* value of 51.62 kJ mol^{-1} K^{-1}. Accumulation of the equilibrium intermediates is not the sole reason for the low *m* value of protein unfolding (*58*). The other reasons may be (i) the presence of the residual structure of the unfolded state (*59, 60*), (ii) the extended chalice-like conformation of the native state of full-length IF2 with the accessible surface area being larger than the surface of a tightly packed globular protein with a similar molecular mass, and (iii) parallel independent unfolding of the domains. Most likely, all three reasons mentioned here influence, in concert, the low experimentally determined low *m* value of full-length IF2. Moreover, the existence of partial unfolding of the native state of IF2wt cannot be excluded. In fact, natively (partially) unfolded proteins were thought to participate in many critical cellular control mechanisms and processes such as the initiation of translation (*61, 62*).

The presence of equilibrium intermediates was also revealed by isothermal denaturation analysis and the phase diagram method (Figures 3 and 4). The decrease in the accessible area due to the chalice-like structure may be quantitatively estimated. The accessible surface area of the native state of full-length IF2 is larger than in an average protein, implying a smaller ΔASA_{unf} and consequently a smaller *m* value than expected. The accessible surface area of tightly packed native globular proteins is dependent on the molecular weight: $ASA_{native} = 11.1 \times M^{2/3}$ (*63*). Using this relation, we have calculated the accessible surface area for IF2/eIF5B from *M. thermoautotrophicum* to be 18610 Å^2 (*20*). On the basis of the crystal structure, ASA_{native} = 26440 Å^2, which decreases the *m* value by only ∼1.7 kJ mol^{-1} K^{-1}. This indicates the involvement of other factors in the low observed *m* value. Analogously, the prediction of changes in the accessible surface area for IF2G is 32667 Å^2 and for IF2C 18623 Å^2, yielding *m* values of 33.7 and 20.75 kJ mol^{-1} K^{-1}, respectively. The experimentally determined *m* values of 11.6 ± 0.6 and 8.4 ± 0.4 kJ mol^{-1} K^{-1} for IF2G and IF2C, respectively, indicate the existence of intermediates in isothermal chemical unfolding of both domains. In agreement with our findings from analysis of isothermal denaturation, the C-terminal domain of IF2 from *B. stearothermophilus* shows three-state unfolding (*13*). However, alternative analysis by the phase diagram method indicates four-state unfolding. Misselwitz et al. suggested that the C-terminal domain consists of two subdomains of unequal stability. In accordance with their interpretation and in agreement with the high level of sequence similarity of both proteins, we also conclude that the C-terminal domain of *T. thermophilus* IF2 consists of two subdomains. The presence of an extra intermediate, observed in the phase diagram, is probably related to weakening of domain−domain interactions within the C-terminal domain. However, unfolding of these subdomains in IF2 from *T. thermophilus* is cooperative, indicating that their structure is more compact. Strong resistance to proteolysis further confirms the remarkable compactness of the C-terminal domain of *T. thermophilus* IF2 (*11*).

Interestingly, all $[GdnHCl]_{1/2}$ values defined as $\Delta G°/m$ for IF2wt, IF2G, and IF2C equal ∼4.0 M. This demonstrates that the unfolding of the whole protein, as well as its separate domains, proceeds at the same GdnHCl concentration, pointing out the cooperativity of the transition. Unfortunately, the presence of equilibrium intermediates in the unfolding of IF2wt, IF2G, and IF2C prevents us from assessing the interaction energy between domains from the comparison of their apparent free energies of unfolding. Nevertheless, the fluorescence dependences for IF2wt and individual domains are very similar, indicating an absence of domain interactions in the cooperativity of unfolding. Isothermal denaturation of IF2wt and its domains revealed its strong resistance to the denaturation effect of urea. Consistent with the positions of the emission maxima of the tryptophan fluorescence at ∼340 nm, even in the presence of 9 M urea,

IF2wt and its domains preserved the native-like secondary structures with only slightly perturbed tertiary structures (*64*).

Reversibility of the Thermal Transition of IF2wt and Its Isolated Domains. IF2 from *T. thermophilus* represents one of the largest proteins with the ability of reversible refolding after thermal denaturation in vitro. The high reversibility of the thermal denaturation of multidomain IF2 raises the question of whether isolated domains are capable of refolding into their native states. Individual domains could represent autonomous folding units and, upon refolding, would reconstitute into their native conformation. This possibility seems plausible, as the X-ray structure of IF2/eIF5B reveals only a few domain−domain contacts. In this case, the reversibility of the thermal denaturation of isolated domains should be similar to that of intact IF2. Our results showed that the transition temperature of IF2G is very similar to that of the intact protein. On the other hand, IF2C aggregates at high temperatures. The C-terminal domain of *B. stearothermophilus* IF2 studied by DSC at neutral pH also exhibited irreversible aggregation, in accordance with our results. Furthermore, the presence of GdnHCl increased the reversibility of the transition of the *B. stearothermophilus* C-terminal domain (*13*). Formation of the interdomain disulfide bond by two cysteines present in the C-terminal domains of IF2 from *B. stearothermophilus* and *T. thermophilus* may explain the aggregation induced by the thermal denaturation. Sequences of C-terminal domains of *B. stearothermophilus* and *T. thermophilus* IF2 have similar hydrophobicity patterns. The C-terminal domain of *B. stearothermophilus* IF2 (mean value of 0.724) is only slightly more hydrophobic than the C-terminal domain of *T. thermophilus* IF2 (mean value of 0.722). Both isolated G-domains of IF2 with mean values of 0.703 and 0.715 for *B. stearothermophilus* and *T. thermophilus*, respectively, are less hydrophobic than the corresponding C-terminal domains.

The change in the heat capacity of a protein due to thermal denaturation is a suitable parameter for assessing the denaturation state of the protein. A common approach to the determination of changed heat capacity is a plot of ΔH_{cal} versus T_{trs} obtained from measurements in solvent at varying pHs (*65*). However, the transition temperature of IF2wt is independent of pH between 6.0 and 10.5, and the protein tends to aggregate at pH <5.5 (unpublished results). On the other hand, a detailed thermodynamical study of lysozyme denaturation in the presence of a denaturant revealed that the calculated heat capacity change from a ΔH_{cal} versus T_{trs} plot at various GdnHCl concentrations led to a value only slightly lower than that obtained due to pH variation (*66, 67*). Therefore, apparent heat capacity changes were calculated from DSC scans at various GdnHCl concentrations. Due to dimerization of IF2wt and the tendency of IF2C to aggregate, only $\Delta c_{p,app}$ for IF2G was determined. The obtained value of 22.3 ± 2.9 kJ mol^{-1} K^{-1} is in very good accord with the heat capacity change of 24.9 kJ mol^{-1} K^{-1} estimated from the relation between the molecular mass and the change in the accessible surface area (*57*).

Thermal Stability of IF2wt and Its Isolated Domains. Enthalpies and transition temperatures were calculated at various concentrations of GdnHCl (Table 2A−C of the Supporting Information). Surprisingly, the $\Delta H_{vH}/\Delta H_{cal}$ ratio equaled 2 for IF2wt, indicating that the dimer is the cooperative unit of intact IF2 in thermal denaturation. The dependence of the transition temperature on protein concentration accompanies changes in the oligomeric state of a protein in the process of thermal denaturation. However, the transition temperatures of IF2wt measured by DSC and by CD in the near-UV region are nearly the same despite the >10-fold difference in protein concentration. From the fact that $\Delta H_{vH}/\Delta H_{cal}$ is ∼1 for IF2G and from the tendency of IF2C to aggregate, we assume that the dimer observed in thermal denaturation of IF2wt is probably stabilized through intermonomeric interactions between the C-terminal domains. Our results indicate that the G-domain increases the reversibility of the thermal denaturation of the more hydrophobic C-terminal domain. The isolated C-terminal domain tends to irreversibly aggregate in the absence of the G-domain. This may also explain the extremely low value of the calorimetric enthalpy and apparent dimer formation. The calorimetric enthalpy of denaturation of the whole protein is significantly lower than for the G-domain. Theoretically, thermal denaturation of the full-length protein should be, at least, equal to the sum of the calorimetric enthalpy of the individual domains. The association reaction of the C-terminal domain at high temperatures is an exothermic reaction and may partially compensate for the endothermic denaturation reaction. Simple simulations of the heat capacity show that independent exothermic and endothermic transitions increase the ratio of van't Hoff to calorimetric enthalpy. This also demonstrated that the C-domains interact during the themal denaturation. Similarly, dimerization would explain the lower values of ΔH_{cal} of IF2wt versus those of IF2G in accordance with previous observations (*68, 69*). In the effort to directly trap dimer formation of IF2wt at higher temperatures, we have performed glutaraldehyde cross-linking experiments at different temperatures (20, 55, and 90 °C) (data not shown). Unfortunately, obtained results were not conclusive, supposedly due to the low efficiency of glutaraldehyde cross-linking reactions under these conditions. Despite that, we propose the speculative mechanism of thermal denaturation of IF2wt at <2 M GdnHCl shown in Scheme 1.

According to this scheme, IF2wt forms dimers due to the increased temperature and increased hydrophobic effect before thermal denaturation. Dimeric forms of IF2wt remain intact even after thermal denaturation due to the strong interactions between the C-terminal domains of IF2. Recooling leads to refolding and dimer dissociation. Accordingly, the full-length protein folds into the native conformation, and the G-domain contributes to the solubility of the C-domain. This mechanism enables us to explain the observed findings: (i) a $\Delta H_{vH}/\Delta H_{cal}$ of ∼2, indicating a dimeric form of IF2wt in thermal denaturation, (ii) the absence of dependence of T_{trs} on protein concentration, and (iii) a monomeric form of IF2wt before and after thermal denaturation. Further, this mechanism indicates transient interprotein interactions. Once the intact protein has cooled to room temperature, proper folding might be achieved by interdomain−protein and not by intradomain−protein interaction. The existence of the dimeric form of the protein even in the thermally denatured state was previously observed in the case of elongation factor Ts from *T. thermophilus* (*70*).

The Transition Temperature of IF2wt Depends on the Changes in the Nucleotide Status. The apparent affinity constants of 8 × 10^4 and 7 × 10^3 M^{-1} for GDP and GTP,

Scheme 1

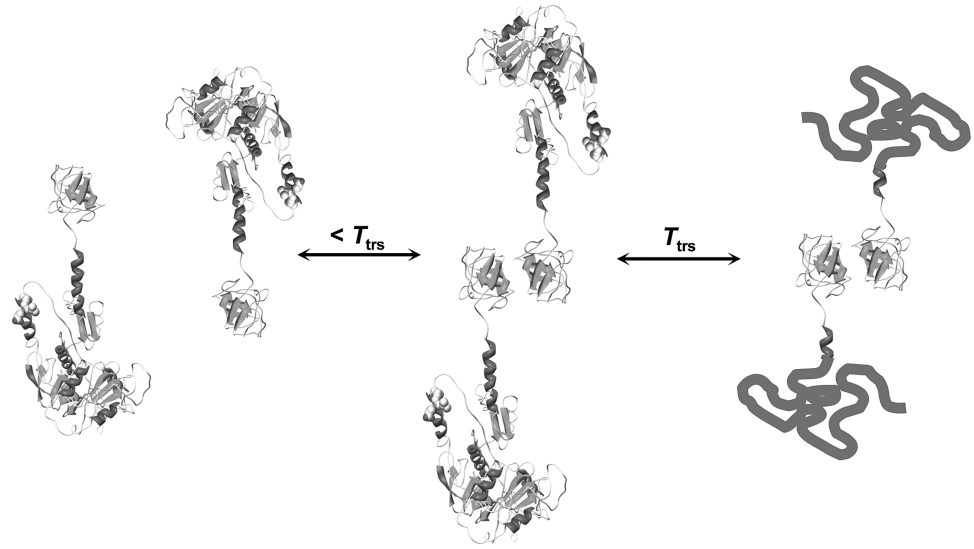

respectively, were determined for the *E. coli* protein at 20 °C. The common binding site of both nucleotides was confirmed by the competitive inhibitory effect of GDP on the formation of the 30S initiation complex in the presence of IF2 and GTP (*7*). Binding of GTP and GDP to IF2 was examined by spectroscopic methods, equilibrium dialysis (*7*), and X-ray structure analysis (*20*). The nucleotide binding site is located in the G-domain which becomes more compact upon binding of the guanine nucleotide triphosphate (*8*). The affinities of the nucleotides for IF2 are lower than in the case of other GTPases involved in the translation of mRNA. Crystal structures of the nucleotide-free, GTP-bound, and GDP-bound forms of IF2 provided insight into molecular details of nucleotide binding (*20*). Nucleotides bind in the shallow hydrophobic pocket surrounded by four loops. Catalytically active Mg^{2+} was found to be stabilized by the conserved threonine residue from the switch 1 effector region. These structural data imply that the native nucleotide-free protein would be stabilized by GDP and GTP binding. Differential scanning microcalorimetry enabled us to show that transition temperatures of the protein are increased in the presence of the guanine nucleotides. The GDP-bound form of the protein is slightly more stable than the IF2·GTP complex. In the presence of 20 mM $MgCl_2$, the transition temperature of the nucleotide-bound IF2 is further increased (data not shown). This implies a role of Mg^{2+} ions in catalysis and in maintenance of protein stability. In analogy with our results with IF2, a DSC study of elongation factor Tu from *T. thermophilus*, performed in the absence and presence of GDP and GTP analogue GppNHp (*71*), demonstrated the higher stability of the GDP-bound form of the protein.

Biological Implications. Thermodynamic parameters for IF2 from *T. thermophilus* obtained from iso/thermal denaturation experiments are in accordance with properties of IF2 homologues in the isolated state (*20*) as well as IF2 from *T. thermophilus* visualized on the ribosome (*56*). (i) IF2 from *T. thermophilus* consists of two multidomain independent parts: G-domain and C-domain. (ii) G- and C-domains in the folded states do not interact with each other (although their interaction might be important in the process of folding). Communication between the domains is mediated by the long α-helix (*20*). (iii) The conformational states of IF2 of *T. thermophilus* in complexes with GDP and GTP analogues are similar (as indicated by close thermal transition temperatures). Hydrolysis of GTP into GDP leads to rotational movements without significant changes in the conformational stability of IF2 (*20, 56*). This conformational change is probably important for dissociation of the IF2−GDP form from the ribosome (*56*). Our analysis indicates that the IF2 atypical chalice-like crystal structure corresponds to the protein conformation in solvent. The ribosome only slightly affects the conformational transition of IF2 from the GTP to GDP form. This is in marked contrast with the case of release factor 2 in which the compact conformation in solvent is significantly affected by binding to the ribosome (*24–27*). A speculative explanation for the unusual extended form in solution in the case of IF2 might be the fact that IF2 binds to the incomplete ribosome, i.e., the 30S ribosomal subunit, while translation takes place within the complete 70S ribosome. Stabilization of a certain conformation of IF2 in the complex with the 30S ribosomal subunit might be incompatible with efficient initiation of translation in bacteria.

ACKNOWLEDGMENT

G.Z. thanks Dr. Garcia-Mira for help with VP-DSC calorimeter and discussions. We thank Dagmar Sedlakova for excellent technical assistance and Dr. LeAnn K. Robinson and Faiza Hussain for editorial help in preparing the manuscript.

SUPPORTING INFORMATION AVAILABLE

GdnHCl-induced isothermal denaturation of IF2wt, IF2G, and IF2C (Figure 1S), tryptophan fluorescence quenching of IF2wt, fluorescence quenching of IF2 from *T. thermophilus* (Figure 2S), distribution of sedimentation coefficients ($s_{20,w}$) of IF2C (Figure 3S), means and variance of all valid solutions of the prediction of secondary structure using CDSSTR (Table 1), and transition temperatures and van't Hoff and calorimetric enthalpies of denaturation at various GdnHCl concentrations for IF2wt (Table 2). This material is available free of charge via the Internet at http://pubs.acs.org.

REFERENCES

1. Travers, A. A., Debenham, P. G., and Pongs, O. (1980) Translation initiation factor 2 alters transcriptional selectivity of *Escherichia coli* ribonucleic acid polymerase. *Biochemistry 19*, 1651–1656.
2. Shiba, K., Ito, K., Nakamura, Y., Dondon, J., and Grunberg-Manago, M. (1986) Altered translation initiation factor 2 in the cold-sensitive ssyG mutant affects protein export in *Escherichia coli*. *EMBO J. 5*, 3001–3006.
3. Caldas, T., Laalami, S., and Richarme, G. (2000) Chaperone properties of bacterial elongation factor EF-G and initiation factor IF2. *J. Biol. Chem. 275*, 855–860.
4. Milon, P., Tischenko, E., Tomsic, J., Caserta, E., Folkers, G., La Teana, A., Rodnina, M. V., Pon, C. L., Boelens, R., and Gualerzi, C. O. (2006) The nucleotide-binding site of bacterial translation initiation factor 2 (IF2) as a metabolic sensor. *Proc. Natl. Acad. Sci. U.S.A. 275*, 13962–13967.
5. Severini, M., Choli, T., La Teana, A., and Gualerzi, C. O. (1990) Proteolysis of *Bacillus stearothermophilus* IF2 and specific protection by GTP. *FEBS Lett. 276*, 14–16.
6. Caserta, E., Tomsic, J., Spurio, R., La Teana, A., Pon, C. L., and Gualerzi, C. O. (2006) Translation initiation factor IF2 interacts with the 30S ribosomal subunit via two separate binding sites. *J. Mol. Biol. 362*, 787–799.
7. Pon, C. L., Paci, M., Pawlik, R. T., and Gualerzi, C. O. (1985) Structure-function relationship in *Escherichia coli* initiation factors. Biochemical and biophysical characterization of the interaction between IF-2 and guanosine nucleotides. *J. Biol. Chem. 260*, 8918–8924.
8. Gualerzi, C. O., Severini, M., Spurio, R., La Teana, A., and Pon, C. L. (1991) Molecular dissection of translation initiation factor IF2. Evidence for two structural and functional domains. *J. Biol. Chem. 266*, 16356–16362.
9. Moreno, J. M., Kildsgaard, J., Siwanowicz, I., Mortensen, K. K., and Sperling-Petersen, H. U. (1998) Binding of *Escherichia coli* initiation factor IF2 to 30S ribosomal subunits: A functional role for the N-terminus of the factor. *Biochem. Biophys. Res. Commun. 252*, 465–471.
10. Krafft, C., Diehl, A., Laettig, S., Behlke, J., Heinemann, U., Pon, C. L., Gualerzi, C. O., and Welfle, H. (2000) Interaction of fMet-tRNA(fMet) with the C-terminal domain of translational initiation factor IF2 from *Bacillus stearothermophilus*. *FEBS Lett. 471*, 128–132.
11. Szkaradkiewicz, K., Zuleeg, T., Limmer, S., and Sprinzl, M. (2000) Interaction of fMet-tRNAfMet and fMet-AMP with the C-terminal domain of *Thermus thermophilus* translation initiation factor 2. *Eur. J. Biochem. 267*, 4290–4299.
12. Spurio, R., Brandi, L., Caserta, E., Pon, C. L., Gualerzi, C. O., Misselwitz, R., Krafft, C., Welfle, K., and Welfle, H. (2000) The C-terminal subdomain (IF2 C-2) contains the entire fMet-tRNA binding site of initiation factor IF2. *J. Biol. Chem. 275*, 2447–2454.
13. Misselwitz, R., Welfe, K., Krafft, C., Gualerzi, C. O., and Welfle, H. (1997) Translational initiation factor IF2 from *Bacillus stearothermophilus*: A spectroscopic and microcalorimetric study of the C-domain. *Biochemistry 36*, 3170–3178.
14. Meunier, S., Spurio, R., Czisch, M., Wechselberger, R., Guenneugues, M., Gualerzi, C. O., and Boelens, R. (2000) Structure of the fMet-tRNA^{fMet}-binding domain of *B. stearothermophilus* initiation factor IF2. *EMBO J. 19*, 1918–1926.
15. Wienk, H., Tomaselli, S., Bernard, C., Spurio, R., Picone, D., Gualerzi, C. O., and Boelens, R. (2005) Solution structure of the C1-subdomain of *Bacillus stearothermophilus* translation initiation factor IF2. *Protein Sci. 14*, 2461–2468.
16. Sander, C., and Schneider, R. (1991) Database of homology-derived protein structures and the structural meaning of sequence alignment. *Proteins 9*, 56–68.
17. Kyrpides, N. C., and Woese, C. R. (1998) Universally conserved translation initiation factors. *Proc. Natl. Acad. Sci. U.S.A. 95*, 224–228.
18. Roll-Mecak, A., Shin, B. S., Dever, T. E., and Burley, S. K. (2001) Engaging the ribosome: Universal IFs of translation. *Trends Biochem. Sci. 26*, 705–709.
19. Brock, S., Szkaradkiewicz, K., and Sprinzl, M. (1998) Initiation factors of protein biosynthesis in bacteria and their structural relationship to elongation and termination factors. *Mol. Microbiol. 29*, 409–417.
20. Roll-Mecak, A., Cao, C., Dever, T. E., and Burley, S. K. (2000) X-ray structures of the universal translation initiation factor IF2/eIF5B: Conformational changes on GDP and GTP binding. *Cell 103*, 781–792.
21. Moreno, J. M., Sorensen, H. P., Mortensen, K. K., and Sperling-Petersen, H. U. (2000) Macromolecular mimicry in translation initiation: A model for the initiation factor IF2 on the ribosome. *IUBMB Life 50*, 347–354.
22. Marzi, S., Knight, W., Brandi, L., Caserta, E., Soboleva, N., Hill, W. E., Gualerzi, C. O., and Lodmell, J. S. (2003) Ribosomal localization of translation initiation factor IF2. *RNA 9*, 958–969.
23. Laursen, B. S., Kjaergaard, A. C., Mortensen, K. K., Hoffman, D. W., and Sperling-Petersen, H. U. (2004) The N-terminal domain (IF2N) of bacterial translation initiation factor IF2 is connected to the conserved C-terminal domains by a flexible linker. *Protein Sci. 13*, 230–239.
24. Vestergaard, B., Van, L. B., Andersen, G. R., Nyborg, J., Buckingham, R. H., and Kjeldgaard, M. (2001) Bacterial polypeptide release factor RF2 is structurally distinct from eukaryotic eRF1. *Mol. Cell 8*, 1375–1382.
25. Zoldak, G., Redecke, L., Svergun, D., Konarev, P., Vörtler, S., Dobbek, H., Sedlak, E., and Sprinzl, M. (2006) Release Factors 2 from *Escherichia coli* and *Thermus thermophilus*: Structural, spectroscopic and microcalorimetric studies. *Nucleic Acids Res. 35*, 1343–1353.
26. Rawat, U. B., Zavialov, A. V., Sengupta, J., Valle, M., Grassucci, R. A., Linde, J., Vestergaard, B., Ehrenberg, M., and Frank, J. (2003) A cryo-electron microscopic study of ribosome-bound termination factor RF2. *Nature 421*, 87–90.
27. Klaholz, B. P., Pape, T., Zavialov, A. V., Myasnikov, A. G., Orlova, E. V., Vestergaard, B., Ehrenberg, M., and van Heel, M. (2003) Structure of the *Escherichia coli* ribosomal termination complex with release factor 2. *Nature 421*, 90–94.
28. Pace, C. N., Vajdos, F., Fee, L., Grimsley, G., and Gray, T. (1995) How to measure and predict the molar absorption coefficient of a protein. *Protein Sci. 4*, 2411–2423.
29. Pace, C. N. (1986) Determination and analysis of urea and guanidine hydrochloride denaturation curves. *Methods Enzymol. 131*, 266–280.
30. Vornlocher, H. P., Scheible, W. R., Faulhammer, H. G., and Sprinzl, M. (1997) Identification and purification of translation initiation factor 2 (IF2) from *Thermus thermophilus*. *Eur. J. Biochem. 243*, 66–71.
31. Eftink, M. R., and Ghiron, C. A. (1981) Fluorescence quenching studies with proteins. *Anal. Biochem. 114*, 199–227.
32. Sanchez-Ruiz, J. M. (1995) Differential scanning calorimetry of proteins. *Subcell. Biochem. 24*, 133–176.
33. Sturtevant, J. M. (1987) Biochemical applications of differential scanning calorimetry. *Annu. Rev. Phys. Chem. 38*, 463–488.
34. van Holde, K. E., and Weischet, W. O. (1978) Boundary Analysis of Sedimentation-Velocity Experiments with Monodisperse and Paucidisperse Solutes. *Biopolymers 17*, 1387–1403.
35. Bates, P. A., and Sternberg, M. J. E. (1999) Model Building by Comparison at CASP3: Using Expert Knowledge and Computer Automation. *Proteins 3* (Suppl.), 47–54.
36. Bates, P. A., Kelley, L. A., MacCallum, R. M., and Sternberg, M. J. E. (2001) Enhancement of Protein Modelling by Human Intervention in Applying the Automatic Programs 3D-JIGSAW and 3D-PSSM. *Proteins 5* (Suppl.), 39–46.
37. Lobley, A., Whitmore, L., and Wallace, B. A. (2002) DICHROWEB: An interactive website for the analysis of protein secondary structure from circular dichroism spectra. *Bioinformatics 18*, 211–212.
38. Whitmore, L., and Wallace, B. A. (2004) DICHROWEB, an online server for protein secondary structure analyses from circular dichroism spectroscopic data. *Nucleic Acids Res. 1*, 32.
39. Mao, D., Wachter, E., and Wallace, B. A. (1982) Folding of the mitochondrial proton adenosinetriphosphatase proteolipid channel in phospholipid vesicles. *Biochemistry 21*, 4960–4968.
40. Shi, Z., Woody, R. W., and Kallenbach, N. R. (2002) Is polyproline II a major backbone conformation in unfolded proteins? *Adv. Protein Chem. 62*, 163–240.
41. Park, S. H., Shalongo, W., and Stellwagen, E. (1997) The role of PII conformations in the calculation of peptide fractional helix content. *Protein Sci. 6*, 1694–1700.
42. Bienkiewicz, E. A., Woody, M. A., and Woody, R. W. (2000) Conformation of the RNA polymerase II C-terminal domain: Circular dichroism of long and short fragments. *J. Mol. Biol. 297*, 119–133.

43. Ionescu, R. M., and Eftink, M. R. (1997) Global analysis of the acid-induced and urea-induced unfolding of staphylococcal nuclease and two of its variants. *Biochemistry 36*, 1129–1140.
44. Kuznetsova, I. M., Stepanenko, O. V., Turoverov, K. K., Zhu, L., Zhou, J. M., Fink, A. L., and Uversky, V. N. (2002) Unraveling multistate unfolding of rabbit muscle creatine kinase. *Biochim. Biophys. Acta 1596*, 138–155.
45. Kuznetsova, I. M., Turoverov, K. K., and Uversky, V. N. (2004) Use of the phase diagram method to analyze the protein unfolding-refolding reactions: Fishing out the "invisible" intermediates. *J. Proteome Res. 3*, 485–494.
46. Bushmarina, N. A., Kuznetsova, I. M., Biktashev, A. G., Turoverov, K. K., and and Uversky, V. N. (2001) Partially folded conformations in the folding pathway of bovine carbonic anhydrase II: A fluorescence spectroscopic analysis. *ChemBioChem 2*, 813–821.
47. Chen, K., Liu, Z., and Kallenbach, N. R. (2004) The polyproline II conformation in short alanine peptides is noncooperative. *Proc. Natl. Acad. Sci. U.S.A. 101*, 15352–15357.
48. Hamburger, J. B., Ferreon, J. C., Whitten, S. T., and Hilser, V. J. (2004) Thermodynamic mechanism and consequences of the polyproline II (PII) structural bias in the denatured states of proteins. *Biochemistry 43*, 9790–9799.
49. Robertson, A. D., and Murphy, K. P. (1997) Protein structure and the energetics of protein stability. *Chem. Rev. 97*, 1251–1268.
50. Schuck, P. (2000) Size distribution analysis of macromolecules by sedimentation velocity ultracentrifugation and Lamm equation modeling. *Biophys. J. 78*, 1606–1619.
51. Musatov, A., Ortega-Lopez, J., Demeler, B., Osborne, J. P., Gennis, R. B., and Robinson, N. C. (1999) Detergent-solubilized *Escherichia coli* cytochrome bo_3 ubiquinol oxidase: A monomeric, not a dimeric complex. *FEBS Lett. 457*, 153–156.
52. Musatov, A., and Robinson, N. C. (2002) Cholate-induced dimerization of detergent- or phospholipid-solubilized bovine cytochrome *c* oxidase. *Biochemistry 41*, 4371–4376.
53. Stanicova, J., Sedlak, E., Musatov, A., and Robinson, N. C. (2007) Differential stability of dimeric and monomeric cytochrome *c* oxidase exposed to elevated hydrostatic pressure. *Biochemistry 46*, 7146–7152.
54. Laursen, B. S., Mortensen, K. K., Sperling-Petersen, H. U., and Hoffman, D. W. (2003) A conserved structural motif at the N-terminus of bacterial translation initiation factor IF2. *J. Biol. Chem. 278*, 16320–16328.
55. Allen, G. S., Zavialov, A., Gursky, R., Ehrenberg, M., and Frank, J. (2005) The cryo-EM structure of a translation initiation complex from *Escherichia coli*. *Cell 121*, 703–712.
56. Myasnikov, A. G., Marzi, S., Simonetti, A., Giuliodori, A. M., Gualerzi, C. O., Yusupova, G., Yusupov, M., and Klaholz, B. P. (2005) Conformational transition of initiation factor 2 from the GTP- to GDP-bound state visualized on the ribosome. *Nat. Struct. Mol. Biol. 12*, 1145–1149.
57. Myers, J. K., Pace, C. N., and Scholtz, J. M. (1995) Denaturant m values and heat capacity changes: Relation to changes in accessible surface areas of protein unfolding. *Protein Sci. 4*, 2138–2148.
58. Soulages, J. L. (1998) Chemical denaturation: Potential impact of undetected intermediates in the free energy of unfolding and m-values obtained from a two-state assumption. *Biophys. J. 75*, 484–492.
59. Baskakov, I. V., and Bolen, D. W. (1998) Monitoring the sizes of denatured ensembles of staphylococcal nuclease proteins: Implications regarding m values, intermediates, and thermodynamics. *Biochemistry 37*, 18010–18017.
60. Baskakov, I. V., and Bolen, D. W. (1999) The paradox between m values and ΔCp's for denaturation of ribonuclease T1 with disulfide bonds intact and broken. *Protein Sci. 8*, 1314–1319.
61. Wright, P. E., and Dyson, H. J. (1999) Intrinsically unstructured proteins: Re-assessing the protein structure-function paradigm. *J. Mol. Biol. 293*, 321–331.
62. Uversky, V. N., Oldfield, C. J., and Dunker, A. K. (2005) Showing your ID: Intrinsic disorder as an ID for recognition, regulation and cell signaling. *J. Mol. Recognit. 18*, 343–384.
63. Janin, J. (1976) Surface area of globular proteins. *J. Mol. Biol. 105*, 13–14.
64. Burstein, E. A., Vedenkina, N. S., and Ivkova, M. N. (1973) Fluorescence and the location of tryptophan residues in protein molecules. *Photochem. Photobiol. 18*, 263–279.
65. Privalov, P. L. (1979) Stability of proteins: Small globular proteins. *Adv. Protein Chem. 33*, 167–241.
66. Pfeil, W., and Privalov, P. L. (1976) Thermodynamic investigations of proteins. II. Calorimetric study of lysozyme denaturation by guanidine hydrochloride. *Biophys. Chem. 4*, 33–40.
67. Makhatadze, G. I., and Privalov, P. L. (1992) Protein interactions with urea and guanidinium chloride. A calorimetric study. *J. Mol. Biol. 226*, 491–505.
68. Makhatadze, G. I., and Marahiel, M. A. (1994) Effect of pH and phosphate ions on self-association properties of the major cold-shock protein from *Bacillus subtilis*. *Protein Sci. 3*, 2144–2147.
69. Valusova, E., Sedlak, E., Antalik, M., Nock, S., and Sprinzl, M. (2001) Effect of N-domain on the stability of elongation factor Ts from *Thermus thermophilus*. *Biochim. Biophys. Acta 1547*, 117–126.
70. Sedlak, E., Valusova, E., Nesper-Brock, M., Antalik, M., and Sprinzl, M. (2001) Effect of the central disulfide bond on the unfolding behavior of elongation factor Ts homodimer from *Thermus thermophilus*. *Biochemistry 40*, 9579–9586.
71. Sedlak, E., Sprinzl, M., Grillenbeck, N., and Antalik, M. (2002) Microcalorimetric study of elongation factor Tu from *Thermus thermophilus* in nucleotide-free, GDP and GTP forms and in the presence of elongation factor Ts. *Biochim. Biophys. Acta 1596*, 357–365.

BI702295G